Supporting Information

Hybrid lipoplex co-delivering siPD-L1/miR-140-5p reverses T cell exhaustion via post-transcriptional regulation for in situ photothermal vaccination

Qunjie Bi[1], Huan Yang[1], Shiyi Li[1], Haoyue Chen[1], Yichun Wang[1], Binbin Yang[1], Tao Zhang[2], Xia He[3], Matthias Barz[4], Heyang Zhang[4], Rongrong Jin[1]*, Yu Nie[1,2,3]*

1. National Engineering Research Center for Biomaterials, College of Biomedical Engineering, Sichuan University, Chengdu, 610041, China

2. Department of Biochemistry and Molecular Biology, School of Biological Sciences and Technology, Chengdu Medical College, Chengdu 610500, Sichuan, China

3. Department of Pharmacy, Sichuan Academy of Medical Sciences & Sichuan Provincial People's Hospital, School of Medicine, University of Electronic Science and Technology of China, Chengdu, 610072, China

4. Leiden Academic Center for Drug Research (LACDR), Leiden University, Leiden 2333 CC, the Netherlands

*Corresponding authors: nie_yu@scu.edu.cn (Yu Nie); jinrr2015@scu.edu.cn (Rongrong Jin);

1. Acronyms

3'-UTR	3' untranslated region
AR	AuNF coated RLS lipoplexes
AR/si/mi	AuNF/RLS/siRNA/miRNA
ARC	AuNF/RLS/CpG
AuNFs	gold nanoflowers
AuNPs	gold nanospheres
BMDCs	bone marrow-derived dendritic cells
CCK-8	cell counting kit-8
CDS	coding sequence
CpG ODN	CpG oligodeoxynucleotide
DAPI	4′,6-diamidino-2-phenylindole
DCs	dendritic cells
EG.7.OVA	OVA-expressing EL4 murine thymoma cell line
FITC	fluorescein isothiocyanate
HeLa-GFP	Green fluorescent protein (GFP) stable-expressing human cervical carcinoma cell line
ICD	immunogenic cell death
ICIs	immune checkpoint inhibitors

Lipo2000	Lipofectamine 2000
miRNA	microRNA
MPTT	mild photothermal therapy
NIR	Near-infrared
OS	overall survival
OVA	Ovalbumin
PD-L1	programmed cell death ligand 1
PTT	Photothermal treatment
qPCR	quantitative real-time polymerase chain reaction
RIPA	radioimmunoprecipitation assay
RNAi	RNA interference
Rr	pearson correlation coefficient
siGFP	silencing GFP siRNA
siPD-L1	silencing PD-L1 siRNA
siRNA	small interfering RNA
TAAs	tumor-associated antigens
TEM	transmission electron microscope

Table S1. The sequences of siRNA

siRNA	Sense (5’ - 3’)	Antisense (5’ - 3’)
siPD-L1-1	CCCACAUAAAAAACAGUUGTT	CAACUGUUUUUUAUGUGGGTT
siPD-L1-2	UGAGAAAACAAGUGAGAAUTT	AUUCUCACUUGUUUUCUCATT
siPD-L1-3	GAGGUAAUCUGGACAAACATT	UGUUUGUCCAGAUUACCUCTT
siPD-L1-4	AGACGUAAGCAGUGUUGAATT	UUCAACACUGCUUACGUCUTT
siPD-L1-5	GCCGAAGUCAUCUGGACAATT	UUGUCCAGAUGACUUCGGCTT
siPD-L1-6	ACUUCUGAGCAUGAACUAAUAUG	CAUAUUAGUUCAUGCUCAGAAGU

Table S2. The sequences of miRNA

miRNA	Sense (5’ - 3’)	Antisense (5’ - 3’)
miR-17-5p	CAAAGUGCUUACAGUGCAGGUAG	ACCUGCACUGUAAGCACUUUGUU
miR-155-5p	UUAAUGCUAAUUGUGAUAGGGGU	CCCUAUCACAAUUAGCAUUAAUU
miR-142-5p	CAUAAAGUAGAAAGCACUACU	UAGUGCUUUCUACUUUAUGUU
miR-140-5p	CAGUGGUUUUACCCUAUGGUAG	ACCAUAGGGUAAAACCACUGUU

Table S3. The primer sequences for various genes.

Target	Forward primer	Reverse primer
IL-1β	TCGCAGCAGCACATCAACAAGAG	TGCTCATGTCCTCATCCTGGAAGG
TNF-α	GCGACGTGGAACTGGCAGAAG	GCCACAAGCAGGAATGAGAAGAGG
IL-6	AGAGGAGACTTCACAGAGGA	ATCTCTCTGAAGGACTCTGG
PD-L1	CGAGGGTTATCCAGAAGCTGAG	CTGGTCACATTGAGAAGCATCC
β-actin	GTGCTATGTTGCTCTAGACTTCG	ATGCCACAGGATTCCATACC

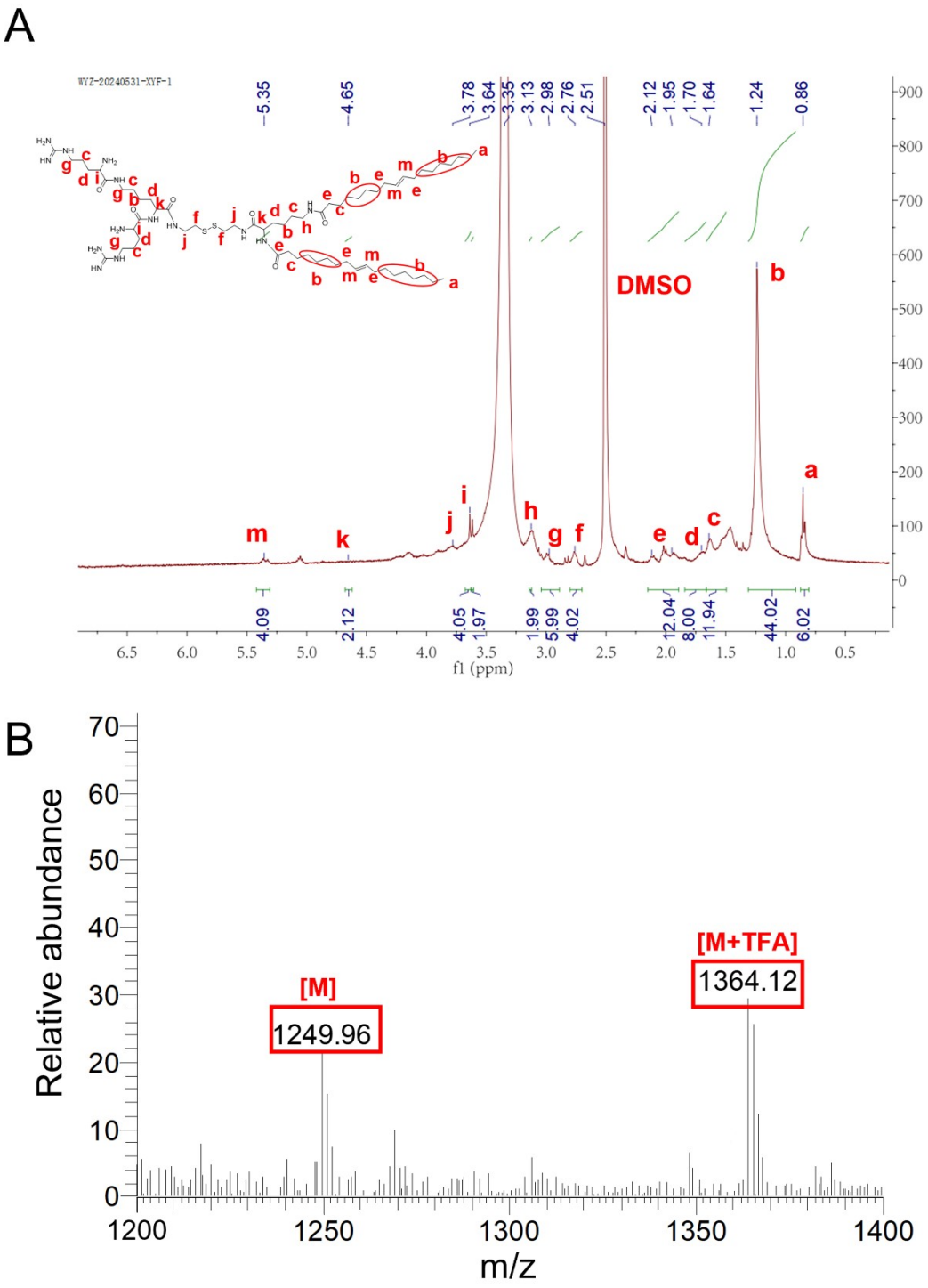

Fig. S1. Chemical characterization (A) ^{1}H NMR spectrum and (B) LC-MS of RLS.

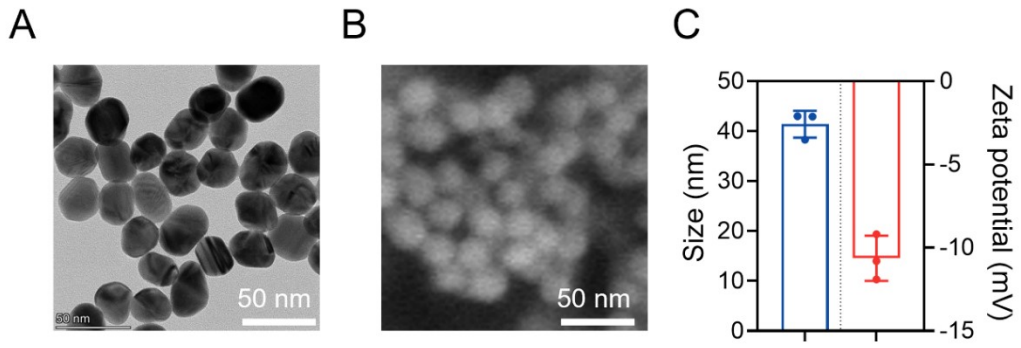

Fig. S2. Characterization of gold nanoparticles. (A) The representative (TEM) image of AuNPs. The scale bar is 50 nm. (B) The representative scanning electron microscope (SEM) image of AuNP. The scale bar is 50 nm. (C) Size distribution and ζ potential of AuNPs as detected by dynamic light scattering (DLS).

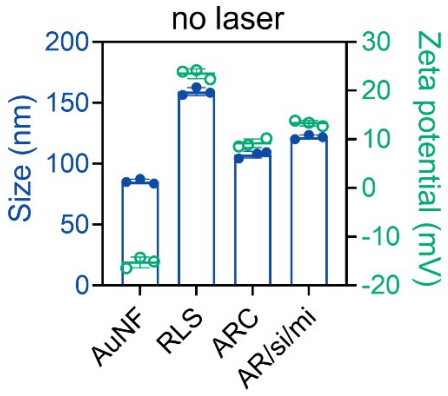

Fig. S3. Size distribution and ζ potential of AuNF, RLS, and hybrid lipoplexes after a mild irradiation condition (808 nm, 1.5 W/cm², 10 min) as detected by dynamic light scattering (DLS). All values represent the mean ± SD (n = 3).

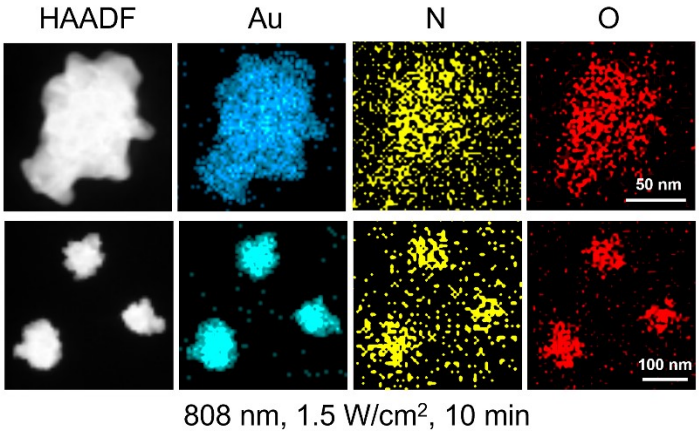

Fig.S4. The HAADF-STEM image of ARC after a mild irradiation condition (808 nm, 1.5 W/cm², 10 min). The scale bar is 50 and 100 nm.

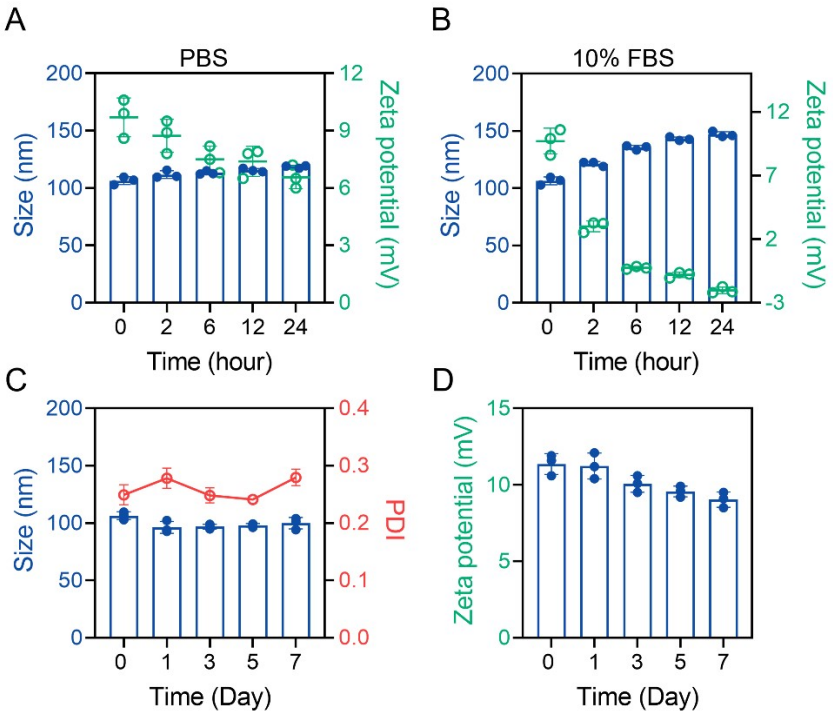

Fig.S5. Stability evaluation of the hybrid lipoplexes. Size distribution and ζ potential of hybrid lipoplexes after incubation in (A) PBS or (B) 10% FBS containing medium at 37 °C for 0, 2, 4, 6, 12 and 24 h as detected by dynamic light scattering (DLS). (C) Size distribution and PDI of hybrid lipoplexes during storage at 4 °C in deionized water for 0, 1, 3, 5 and 7 days. (D) ζ potential of hybrid lipoplexes during storage at 4 °C in deionized water for 0, 1, 3, 5 and 7 days. All values represent the mean ± SD (n = 3).

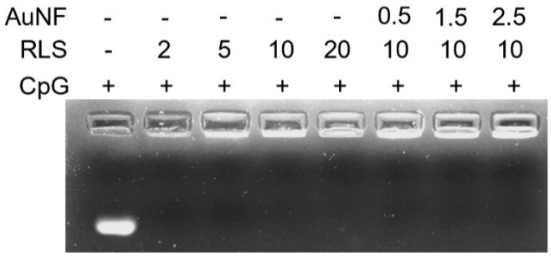

Fig. S6. Gene compaction of ARC at different weight ratios. RLS/CPG at N/P ratios of 1, 2, 5, 10, and 20, and AuNF/CpG at weight ratios of 0.5, 1.5, 2.5.

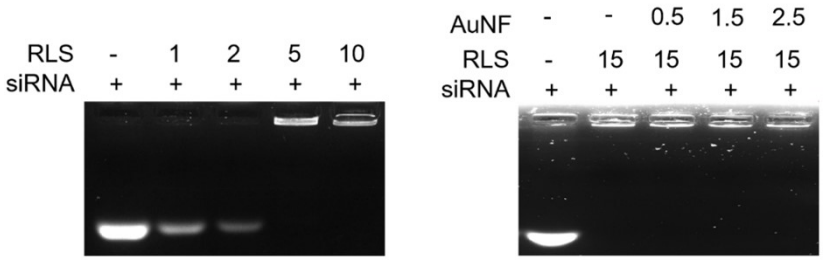

Fig. S7. Gene compaction of RLS/siRNA lipoplexes and AR/siRNA with different mass ratios. (RLS/siRNA at N/P ratios of 1, 2, 5, and 10; and AuNF/siRNA at weight ratios of 0.5, 1.5, 2.5,

siRNA = 0.2 μg).

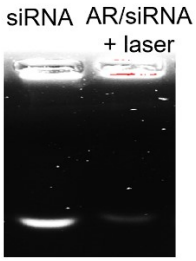

Fig.S8. Gene compaction of AR/siRNA after a mild irradiation condition (808 nm, 1.5 W/cm², 10 min). (siRNA = 0.2 μg, RLS/siRNA at N/P ratio of 15; and AuNF/siRNA at weight ratio of 1.5.)

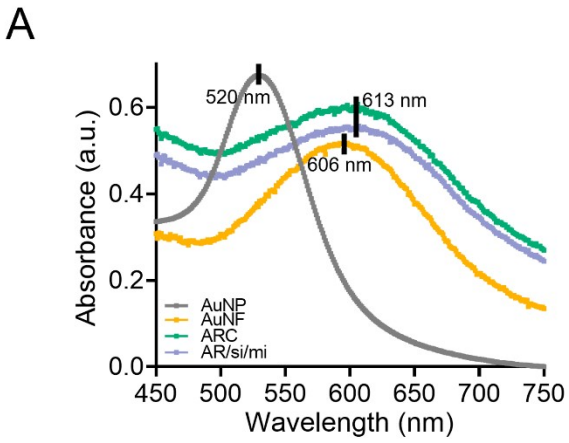

Fig. S9. Ultraviolet-visible spectroscopy (UV-vis) absorption spectra of AuNPs, AuNFs, ARC and AR/si/mi.

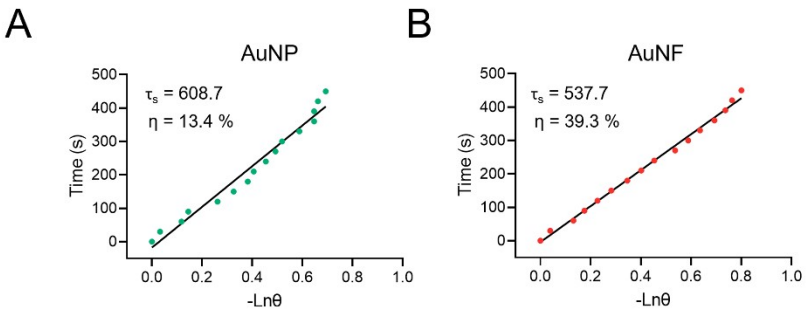

Fig. S10. Evaluation of photothermal conversion efficiency. Calculation time constant (τs) and photothermal-conversion efficiency (η) of (A) AuNPs and (B) AuNFs. Photothermal stability of AuNPs or AuNFs with five cycled irradiations (808 nm, 1.5 W/cm², 10 min) separated by a 20 min cooling phase. Cooling curves used for the determination of the time constant (τs).

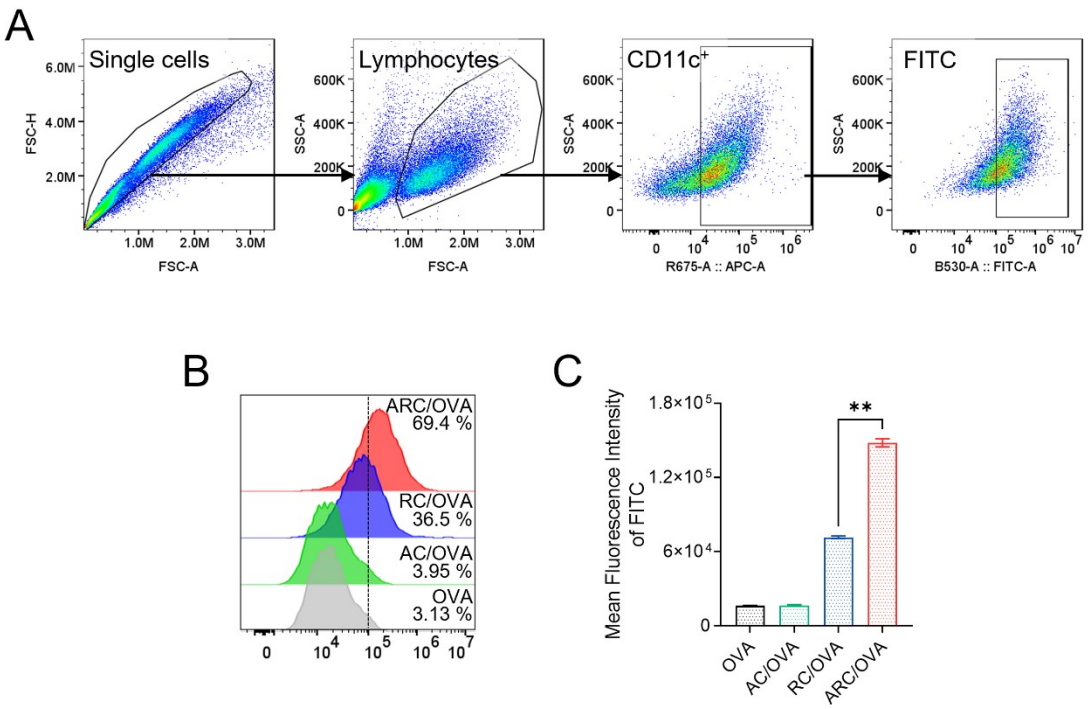

Fig. S11. Cellular uptake of different lipoplexes in BMDCs. (A) Gating strategy for CD11c and FITC-OVA. (B) BMDCs treated with various OVA-loaded lipoplexes for 4 h and the cellular uptake determined by flow cytometer. (C) Quantitative analysis of the cellular uptake of various lipoplexes by MFI. All values represent the mean ± SD (n = 3) and were analyzed by two-sided Student's t-test. $^{**}p < 0.01$.

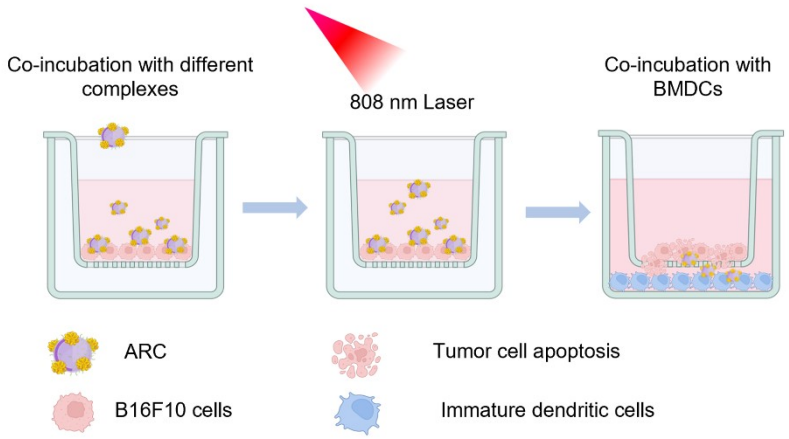

Fig. S12. Schematic illustration of the transwell system experiment. The B16F10 cells were cultured in the upper chamber and irradiated after the addition of different complexes for 4 h (1.5 W/cm², 10 min). Then, the upper chamber was placed into a new lower chamber pre-seeded with BMDCs for a further 20 h. Finally, the BMDCs were harvested for analysis.

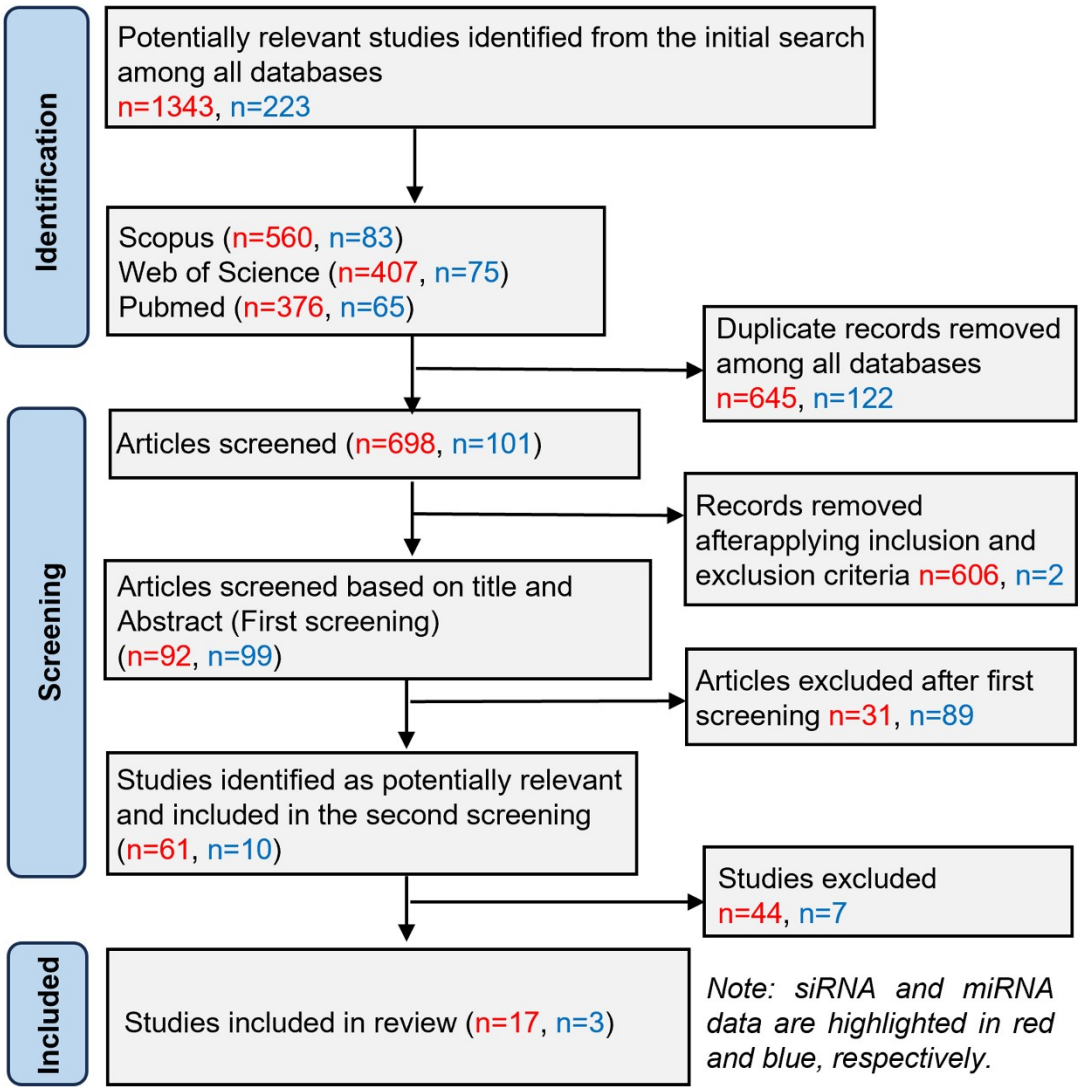

Fig. S13. Flowchart of the literature screening process.

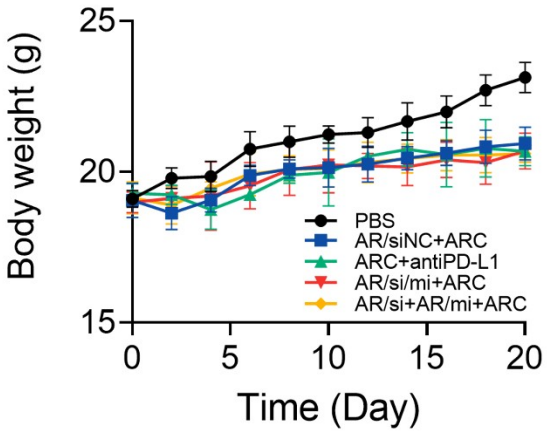

Fig. S14. Body weight change of C57BL/6 mice with B16F10 xenografts in different groups. All values represent the mean ± SD. n = 5 mice.

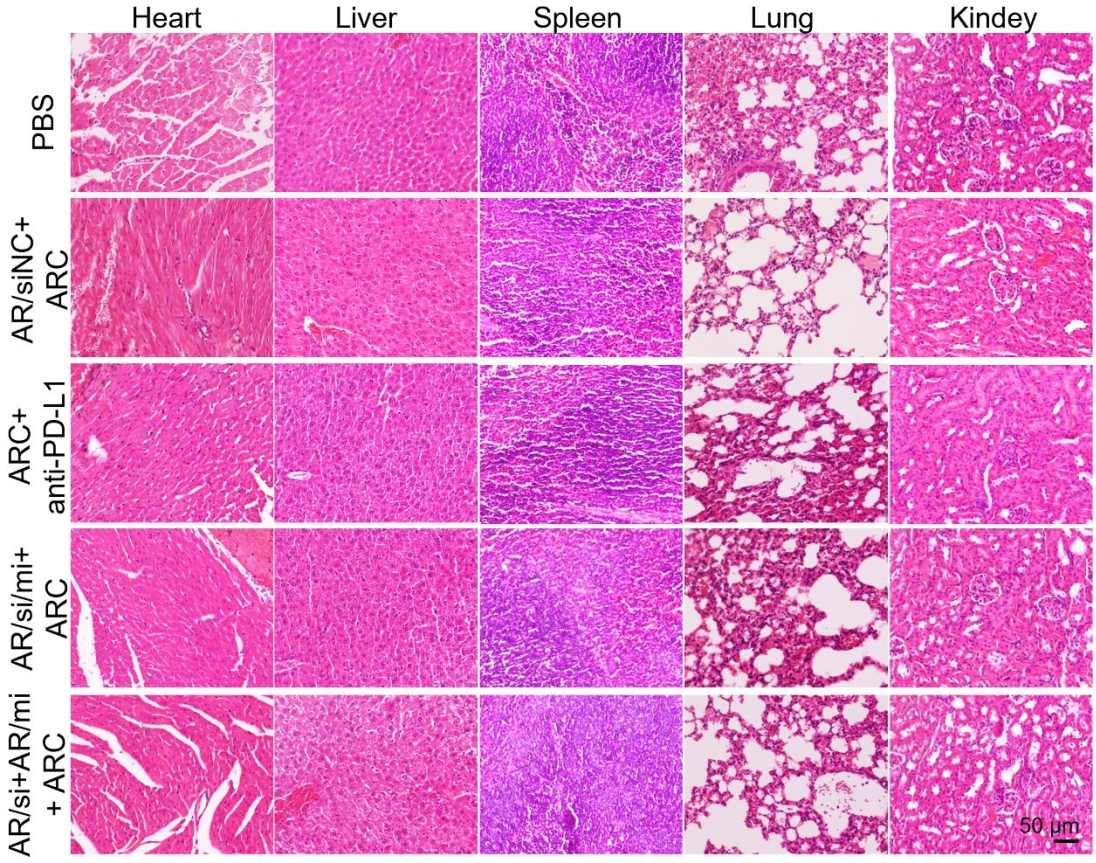

Fig. S15. H&E staining images of major organs of B16F10 tumor-bearing mice after treatment with different lipoplexes. Major organs (including heart, liver, spleen, lung, and kidney) were isolated from the sacrificed mice on day 20. Scale bar is 50 μm.

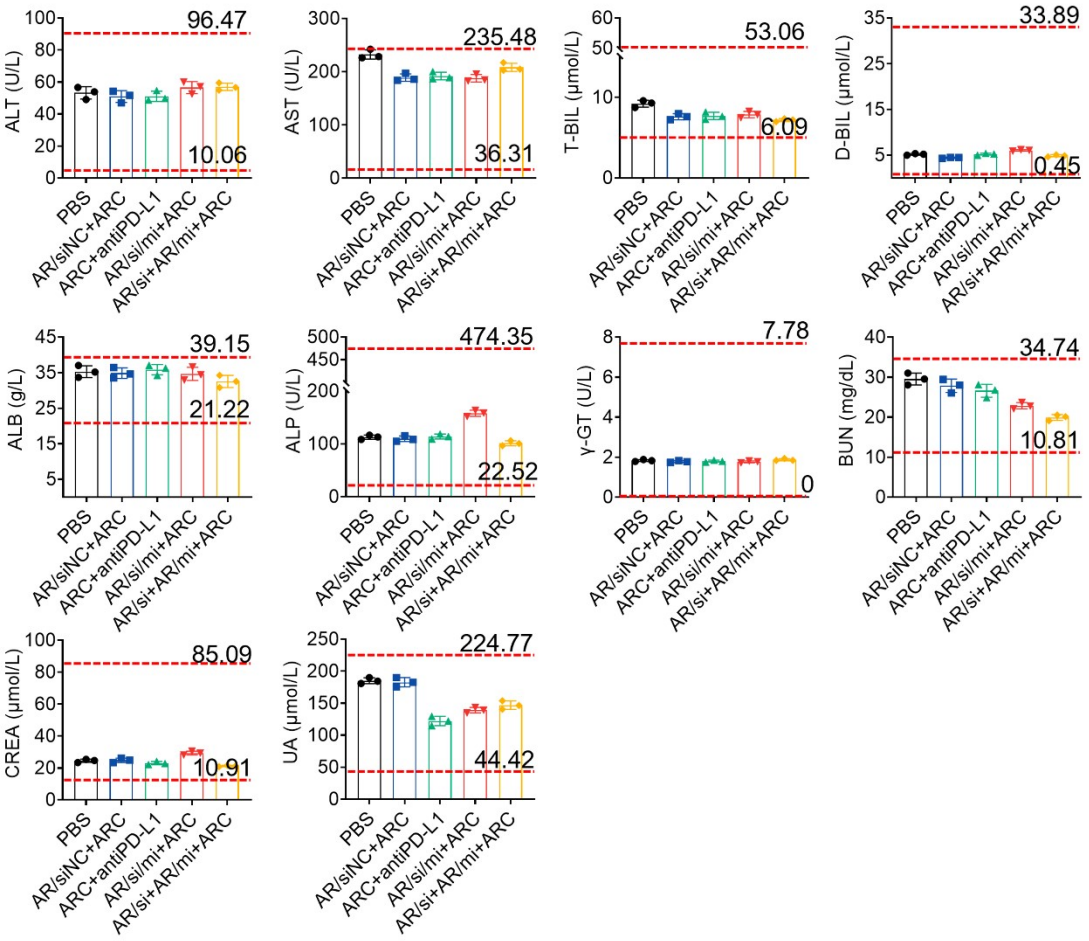

Fig. S16. Hepatic and renal function analyses of B16F10 tumor-bearing mice following different lipoplex administrations. Including alanine aminotransferase (ALT), aspartate aminotransferase (AST), total bilirubin (T-BIL), direct bilirubin (D-BIL), albumin (ALB), alkaline phosphatase (ALP), γ-glutamyl transferase (γ-GT), blood urea nitrogen (BUN), creatinine (CREA), and uric acid (UA). All values represent the mean ± SD (n = 3).

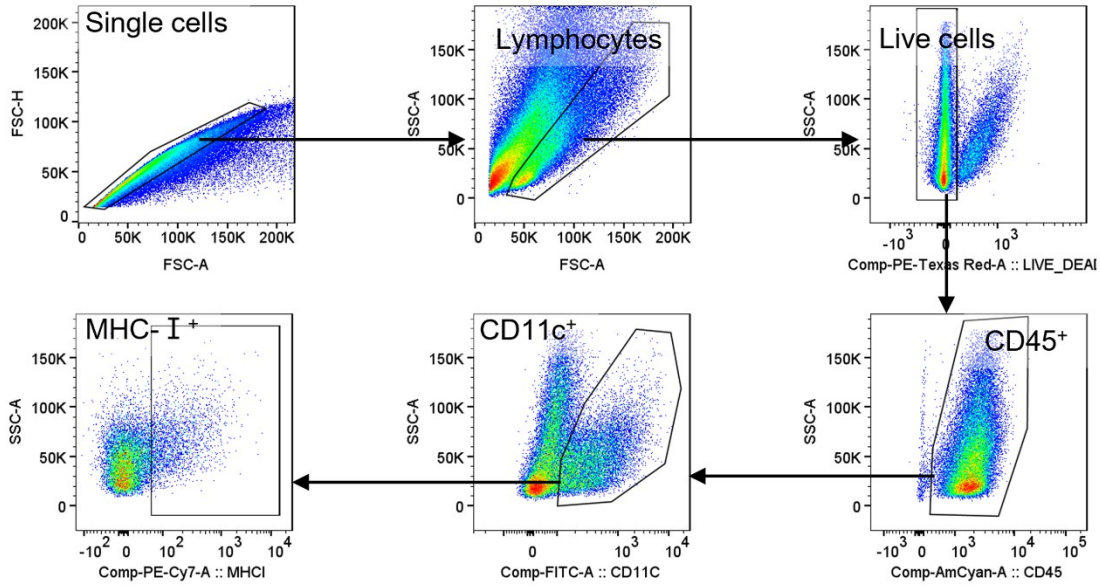

Fig. S17. Gating strategy for identifying BMDC populations within the tumor microenvironment by flow cytometry.

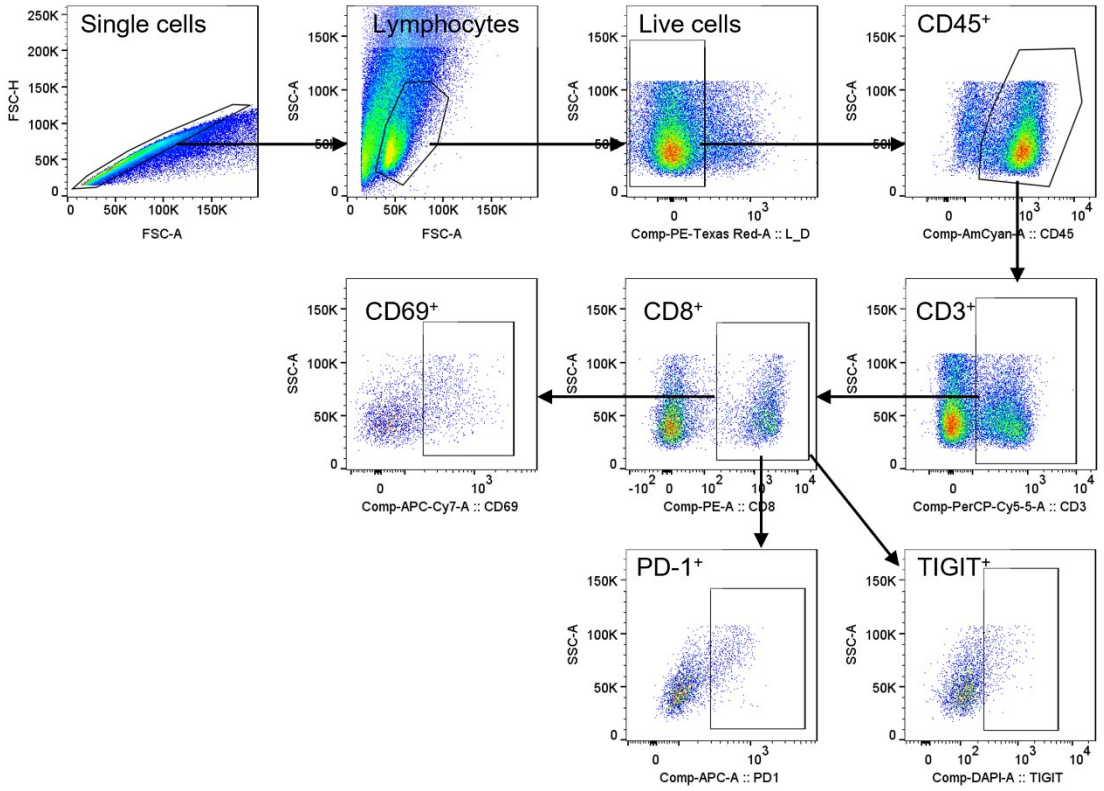

Fig. S18. Gating strategy for identifying T cell populations in the tumor microenvironment by flow cytometry.

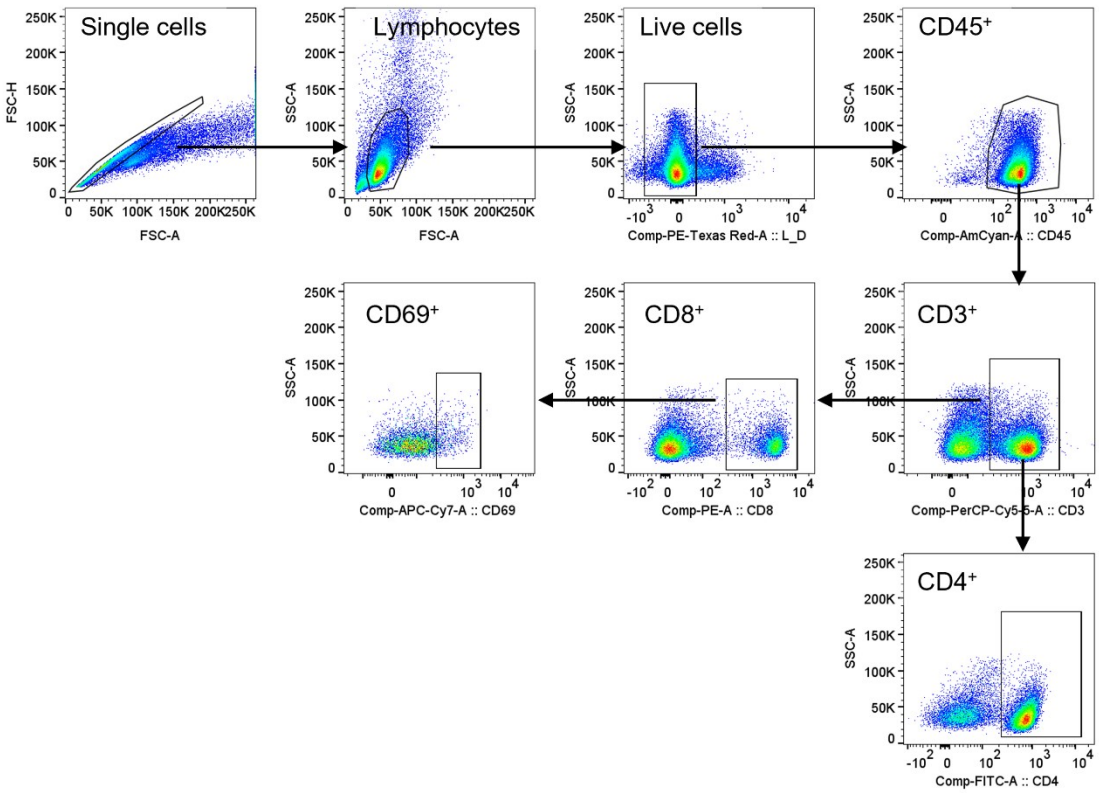

Fig. S19. Gating strategy for identifying immune cell populations in the spleen by flow cytometry.